Electrochemistry Communications 111 (2020) 106666

Contents lists available at ScienceDirect

Electrochemistry Communications

journal homepage: www.elsevier.com/locate/elecom

Label-free analysis of adsorbed protein heterogeneity on individual particles, based on single particle collision events

Wei Yi[a,b], Cong Xu[b,c], Tianyi Xiong[b,c], Tienan Gao[b], Ping Yu[b,c,*], Xiaohua He[a,*], Lanqun Mao[b,c]

[a] School of Chemistry and Molecular Engineering, East China Normal University, 500 Dongchuan Road, Shanghai 200241, China
[b] Beijing National Laboratory for Molecular Sciences, Key Laboratory of Analytical Chemistry for Living Biosystems, Institute of Chemistry, The Chinese Academy of Sciences (CAS), Beijing 100190, China
[c] University of Chinese Academy of Sciences, Beijing 100049, China

ARTICLE INFO

Keywords:
Single particle analysis
Nanopipette
Adsorption heterogeneity
Label-free
Polystyrene particles

ABSTRACT

Investigation of the heterogeneity of protein adsorption on particle surfaces has attracted enormous research attention owing to its great importance in fundamental studies and quality control. Herein we, for the first time, report a new method for label-free analysis of the heterogeneity of protein adsorption on single nanoparticles, based on particle collision events at the orifice of a nanopipette. The dwell time was strongly dependent on the amount of protein adsorbed on polystyrene particles, which could be used to analyze the heterogeneity of protein adsorption at the single particle level. This method presents a label-free, sensitive, reproducible and easily-operated way to analyze adsorption behavior at the single particle level, which opens a new approach to the study of the heterogeneity of physicochemical parameters at the surface of nanoparticles.

1. Introduction

Studying protein adsorption on the surface of particles, especially at the level of a single particle, is of great importance in the fields of nanomedicine [1,2], nanotoxicity [3], and bionic nanomaterials [4]. It is helpful not only in the development of bio-inert drug carriers in the field of biomedicine [5], but also in understanding the binding affinity and stoichiometry between proteins and nanoparticles [6], which directly affect the fate of nanoparticles in vivo. Therefore, monitoring the amount of protein adsorption is necessary for the development of advanced drug delivery systems and efficient analytical quantitative methods since it is strongly related to performance. However, it is a considerable challenge to analyze the amount of protein adsorbed on particle surfaces, mainly due to the complex mechanisms and dynamic nature of protein adsorption processes. Although some techniques (e.g., dynamic light scattering (DLS), transmission electron microscopy (TEM), ultraviolet spectroscopy and fluorescence confocal spectroscopy [7,8]) can provide useful information on protein adsorption, a number of limitations remain. For instance: (1) the requirements of fluorescent labels or drying treatments prohibit the revelation of the actual adsorption state of particles dispersed in solution, and (2) the heterogeneity of the amount adsorbed at the individual particle level can easily be masked by the overall signals provided by these methods. Therefore, label-free analysis of protein adsorption on single particles is still a critical unmet need, and has great potential for studying the heterogeneity of the surface physicochemical parameters of individual particles.

Nanopores, which provide nanoscale confinement for single entities, have been developed as multifunctional platforms for the analysis of single entities at various levels: single molecules [9,10], single particles [11–13], and single cells [14,15]. The principal use of nanopores in testing is usually to amplify the signal induced by the translocation of single entities through the limitations of the structure. Compared with other kinds of solid-state nanopores, glass nanopipettes have a broad range of applications in single particle analysis due to their comparable size, high rigidity and ease of fabrication [16–19]. For example, Long et al. reported a pipette-based label-free method to monitor the immune response of single alpha-fetal proteins (AFP) and the specific antibody [20]. Li et al. demonstrated a novel detection method for microRNA based on resistance-pulse sensing (RPS) single peptide nucleic acid (PNA) modified Fe_3O_4-Au nanoparticles (Fe_3O_4-Au-PNA) with nanopipettes [21]. Moreover, our group has proposed that the counting of phospholipid vesicles could also be achieved using nanopipettes [22].

Unlike traditional RPS methods based on the translocation events of single particles, our group has developed a new single particle detection principle based on the collision events of the particle outside the orifice

* Corresponding authors at: Beijing National Laboratory for Molecular Sciences, Key Laboratory of Analytical Chemistry for Living Biosystems, Institute of Chemistry, The Chinese Academy of Sciences (CAS), Beijing 100190, China (P. Yu).
E-mail addresses: yuping@iccas.ac.cn (P. Yu), xhhe@chem.ecnu.edu.cn (X. He).

https://doi.org/10.1016/j.elecom.2020.106666
Received 10 November 2019; Received in revised form 24 December 2019; Accepted 8 January 2020
Available online 24 January 2020

of a nanopipette [23]. Compared with existing methods for single particle analysis, this method has a number of advantages, including electrochemical activity independence, the fact that it is non-destructive and that it has a weak dependence on nanopipette geometry.

Herein, the heterogeneity of adsorbed proteins on single nanoparticles was investigated based on single particle collision events at the orifice of a nanopipette. Firstly, different amounts of protein (i.e., BSA, bovine serum albumin) were adsorbed on polystyrene (PS) particles by mixing bare PS particles with a BSA solution for different periods of time. It was found that the current drop percentage $\Delta I/I_0$ was almost constant for PS particles with different amounts of protein adsorbed, indicating that the size of the particles was almost the same. However, it was observed that the width of the current drop spike Δt increased with the increased amount of protein adsorption, essentially demonstrating that this method could be used to study the heterogeneity of adsorbed protein on single nanoparticles.

2. Experimental

2.1. Preparation of PS particles adsorbed with different amounts of BSA

A 1.0 mg/mL BSA (Sigma-Aldrich) standard solution was prepared with HAc-NaAc buffer solution (pH 4.7), which was further diluted to different concentrations. The corresponding ultraviolet absorption spectra are shown in Fig. S3a and the absorbance-concentration standard curve is plotted in Fig. S3b, based on the absorbance (OD) of BSA solution at 280 nm. The optimal conditions for BSA adsorption on the PS particles are shown in Fig. S3c–e: the strongest adsorption was achieved in a pH = 4.7, 0.3 mg/mL BSA solution at 30 °C, which are the parameters selected for further experiments. To prepare PS particles with adsorbed BSA (BSA-PS particles), 0.2 mL aqueous solution containing PS particles with a diameter of 500 nm (2.5 wt%, Alfa Aesar) was added into 1.3 mL BSA solution in a centrifuge tube, which was placed in a 30 °C thermostatic oscillator. After constant temperature oscillation (0.5 h, 1 h, 1.5 h, 2 h), the solution was centrifuged (10000 rpm for 5 min) to remove the physically adsorbed BSA, and then dispersed in 0.1 M HAc-NaAc (pH 5.5) buffer solution containing 100 mM KCl. The PS particles with different amounts of adsorbed BSA were used immediately after preparation.

2.2. Characterization of PS particles and PS particles with adsorbed BSA

The morphology of the PS particles was characterized by a SU8020 scanning electron microscopy (HITACHI). TEM imaging of the bare PS particles and BSA-PS particles was performed using a JEM-2010 microscope (JEOL). The zeta potentials of the bare PS particles and BSA-PS particles were measured by a Zetasizer Nano ZS (Malvern Instruments Ltd.).

2.3. Fabrication of nanopipettes

The glass nanopipettes were fabricated using a previously reported protocol. Briefly, borosilicate glass capillaries (1.50 mm O.D. and 0.86 mm I.D., with filament, Sutter Instrument Co.) were first rinsed with piranha solution (30% H_2O_2:98% H_2SO_4 = 3:7) and then with deionized water until neutral. The pretreated capillaries were then further pulled using a P-2000 Laser puller (Sutter Instrument Co., Novato, CA) with the following settings:

heat = 330, filament = 5, velocity = 20, delay = 128, pull = 50
heat = 400, filament = 4, velocity = 15, delay = 130, pull = 175.

The tips of the fabricated nanopipettes were about 150 nm in diameter and the tip geometries were characterized using a SU8020 scanning electron microscope.

2.4. Experimental setup and data analysis

The fabricated nanopipette was filled with and immersed in a 0.1 M HAc-NaAc buffer (pH 5.5) containing 100 mM KCl. One Ag/AgCl electrode was placed in the nanopipette and another in the solution outside the nanopipette (Fig. S1). Current-time curves were obtained by applying a constant voltage between these two electrodes. An Axopatch200B (Molecular Devices) was employed to filter data at 10 kHz, and a Digidata1440A Series (Molecular Devices) was employed to record the signals at a 50 kHz sampling rate. PCLAMP 10 electrophysiological software was used to collect and analyze the raw data. In this experiment, the noise level of the ion current is about 5 pA. Current changes obviously larger than the noise level were considered to be collision signals.

2.5. Finite-element simulations

Finite-element simulations were carried out using COMSOL Multiphysics 5.4 (Comsol, Inc.) on a high-performance workstation to numerically solve the Poisson/Nernst-Planck/Navier-Stokes (PNP-NS) partial differential equations. Simulation details are given in the Supporting Information.

3. Results and discussion

The experimental setup is schematically illustrated in Fig. 1. When BSA-PS particles approached the orifice of the nanopipette, an obvious current transient was observed due to the ion current blockage. Spike signals of different widths were observed owing to the different amounts of adsorbed BSA on the PS particles. The SEM image (Fig. S2a) shows that the average diameter of PS particles without any BSA adsorbed is about 500 nm. The TEM image shows that the BSA-PS particles possessed better dispersion stability (Fig. S2b) as well as improved hydrophilicity (Fig. S2c) compared with bare PS particles; these changes are mainly attributed to BSA adsorption. Furthermore, the current–voltage (I–V) curves of five individual glass nanopipettes prepared in the same program are shown in Fig. S2e. The inner diameter of the nanopipettes was calculated using the formula reported in the literature [24], the inner diameters of the fabricated nanopipettes were calculated to be 157.8 nm, 157.6 nm, 154.9 nm, 160.8 nm and 156.9 nm, respectively. The average inner diameter of nanopipettes was 157.6 ± 2.1 nm. The result of this calculation agreed with the result obtained from a SEM image of the nanopipettes (Fig. S2d).

Fig. 2a shows the typical current–time traces obtained at a nanopipette under 0.6 V. While no obvious spike signal was observed in the absence of PS particles, staircase-type current transients were obtained in the presence of 1.5 pM PS particles, which is consistent with our previous observation (Fig. S4b). By contrast, spike-type current transients were observed for the BSA-PS particles. This difference probably stems from the surface charge differences between the two kinds of particles. To be more specific, the adsorption of BSA reduced the surface charge density of the PS particles. As a result, the electrophoretic force was reduced, causing the particle to escape the orifice in the collision events. The bias potential was kept at 0.6 V to ensure a significant signal-to-noise ratio as well as to prevent the generation of staircase signals under the higher bias. Valid spike-type signals larger than 1 ms were included in the statistics in order to filter the influence of environmental noise (< 1 ms) (Fig. S6) and the signal of the bare PS particles (staircase) (Fig. S4). Two parameters, namely $\Delta I/I_0$ (where ΔI indicates the maximum decrease in current and I_0 refers to the baseline current, see inset in Fig. 2b) and Δt (where Δt was measured as the peak width, see inset in Fig. 2b) are of importance in understanding the current transients. The fitting results in Fig. 2b show that no perceptible difference in $\Delta I/I_0$ was observed as the BSA adsorption time increased from 0.5 h to 2 h, indicating the almost invariable size of the PS particles before and after BSA adsorption, which is consistent with the

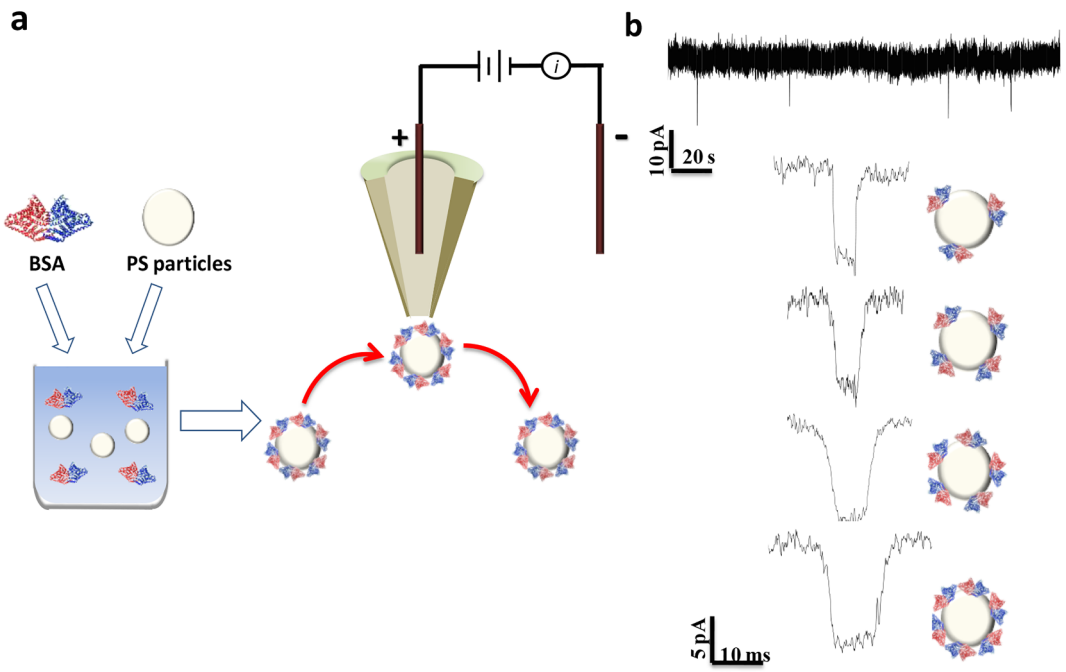

Fig. 1. (a) Schematic illustration of label-free analysis of adsorbed protein heterogeneity on individual particles with a nanopipette. (b) Typical current-time curve and individual event for PS particles adsorbed with different amounts of BSA.

overall results from DLS (Fig. S7). However, significant differences in Δt are observed in the histogram (Fig. 2c). The results in Fig. 2d show that the mean values of Δt at 0.6 V gradually increased with the increase in time, suggesting that the amount of BSA adsorbed on single PS particles was strongly correlated with the mean values of Δt.

Fig. 3a shows that when a 0.6 V bias is applied to the confined

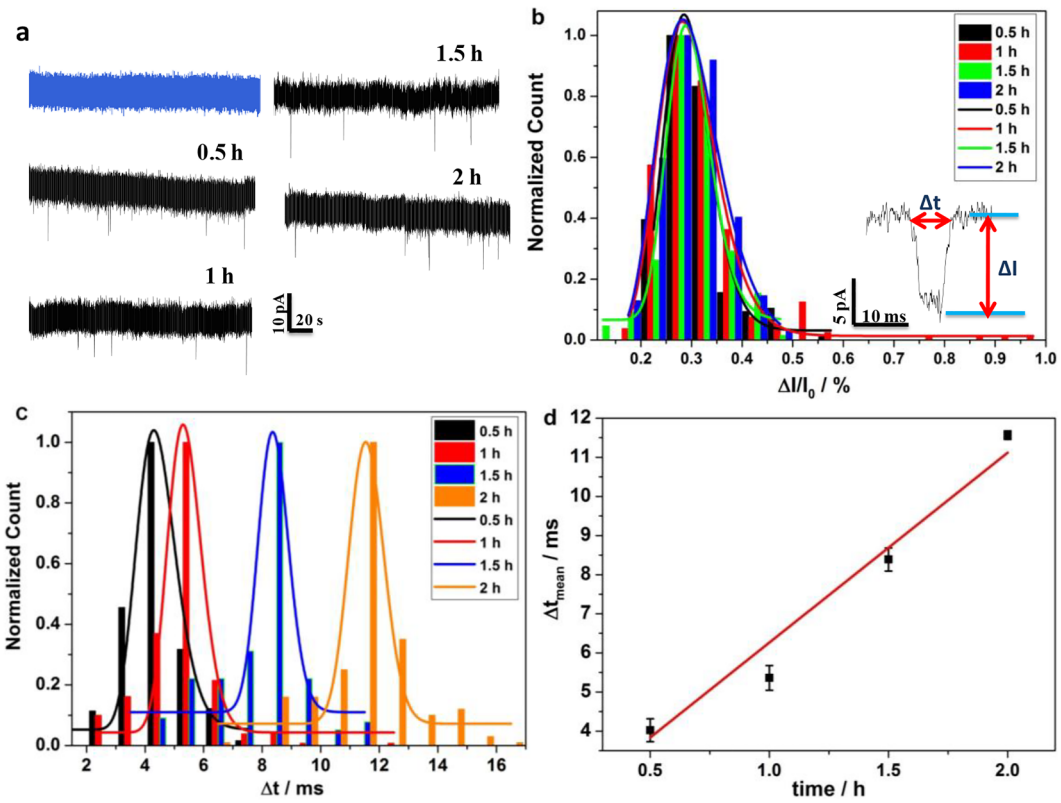

Fig. 2. (a) Typical current-time traces without (blue curve) and with 500 nm-diameter BSA-PS particles for different adsorption times (0.5, 1, 1.5 and 2 h) under a 0.6 V bias potential. (b) Log-normal function fitted results for $\triangle I/I_0$ according to the corresponding histogram distributions at 0.6 V for different BSA adsorption times. The peak transient currents were mainly characterized by the peak height (ΔI) and peak width (Δt) (inset). (c) Log-normal function fitted results for $\triangle t$ according to the corresponding histogram distributions at 0.6 V for different BSA adsorption times. (d) The average dwell time (Δt_{mean}) of PS particles for different BSA adsorption time (0.5, 1, 1.5 and 2 h).

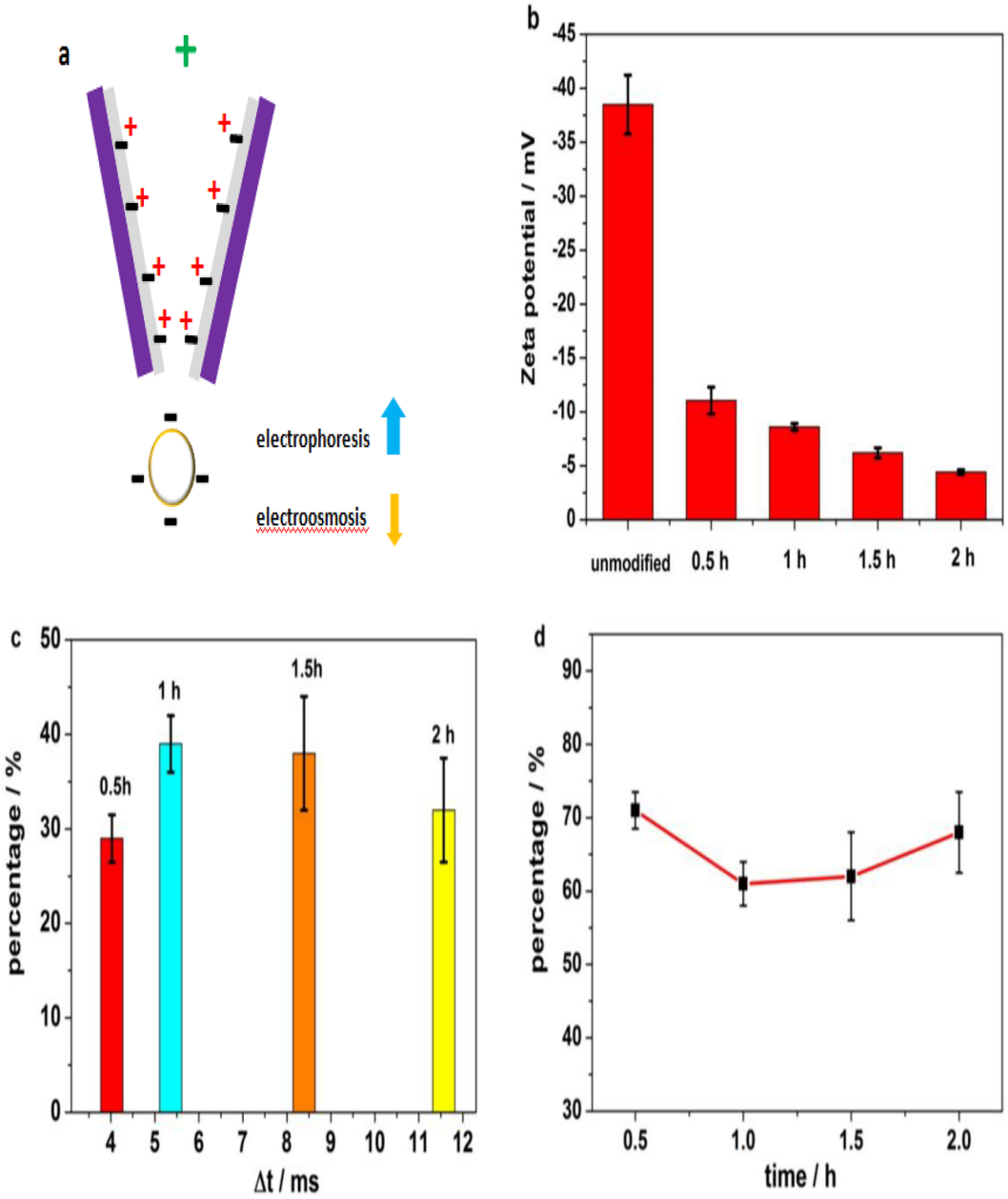

Fig. 3. (a) Schematic illustration of the driving forces on the BSA-PS particle at the orifice of nanopipette. (b) The zeta potential of bare PS particles and BSA-PS particles with different adsorption time (0.5, 1, 1.5 and 2 h) in 0.1 M HAc-NaAc (pH 5.5) buffer solution containing 100 mM KCl. (c) Under different BSA adsorption time, the number of BSA-PS particles within Δt_{mean} ± SD range as a proportion of the total number. (d) The ratio of the number of BSA-PS particles outside the range of Δt_{mean} ± SD to the total number, for different adsorption time.

solution, two electrokinetic forces influence the movement of the negatively charged BSA-PS particles: the forces originating from the electroosmotic flow (EOF) and electrophoresis (EP). While electrophoresis drives the particle to move towards the orifice, the electroosmotic force acts in the opposite direction. To investigate the major factor in these events, a −0.6 V negative bias was applied in the presence of BSA-PS particles in order to invert the direction of EOF and EP. Fig. S5 shows that no pulse signal was observed in the current-time curves at −0.6 V, revealing that EP plays a dominant role in the collision events. In order to further understand the influence of EOF and EP on the ionic current, steady-state finite-element simulations were conducted (Fig. S11), based on the solution of the PNP/NS equations. When the nanoparticle arrives near the orifice of the nanopipette, it blocks the ion flow and thus generates the current transient signals. It is shown that no significant difference was observed with and without consideration of EOF, providing additional evidence that the ionic current is mainly affected by electrophoresis (Fig. S12). The magnitude of the electrophoretic velocity (v_{EP}) can be calculated using the Helmholt–Smoluchowski equation.

$$v_{EP} = \varepsilon_r \varepsilon_o \zeta E/\eta$$

where ε_r is the relative permittivity of the solution, ε_o is the vacuum permittivity of the solution, η is the viscosity of water, E is the magnitude of the electric field at the nanopipette tip, and ζ is the zeta potential of the particles. Based on the above equation, the influence of EP on the particles is related to the electrical field applied to the solution as well as the surface charge characteristics. Since BSA adsorption reduces the surface charge of the PS particles, the particles decelerated, thus causing a longer dwell time which can be observed in the current-time curves. Compared with bare PS particles, the Δt_{mean} of BSA-PS particles

increased from 2.229 ± 0.202 ms to 7.507 ± 0.265 ms under the same experimental conditions (Figs. S8 and S9). The reduction of the driving force of EP also contributed to a reduction in the frequency of collision events. Compared with bare PS particles, a significant reduction in the collision frequency of BSA-PS particles was observed under the same experimental conditions (Fig. S10). The zeta potential of bare PS particles and BSA-PS particles prepared with different BSA adsorption times is shown in Fig. 3b. A significant reduction in surface charge was observed after the adsorption of BSA compared with bare PS particles. Moreover, the zeta potential of PS particles decreases gradually with the increase in adsorption time. As a result, the speed at which particles move in solution becomes slower with the increase in BSA adsorption time, which is consistent with the statistical results for Δt in Fig. 2c. Since the zeta potential data from the instrument and the value of Δt_{mean} (Fig. 2d) given by the nonlinear curve fitting of the Δt statistical value are the average results of numerous single particles, these parameters do not reflect the amount of protein adsorption on each single particle in the solution, but only the average adsorption behavior of PS particles in the solution. Therefore, the uniformity of protein adsorption of PS particles prepared with different BSA adsorption times can be analyzed using the ion current signals from single-particle collisions. The duration of pulsed signals of 500 nm diameter PS particles with different BSA adsorption time (0.5, 1, 1.5 and 2 h) were counted. When the data distribution conforms to the Gaussian distribution, the central tendency measurements can provide us with heterogeneity information about the physicochemical properties of the nanoparticles [25]. As shown in Fig. S13, most of the BSA-PS particles in the statistical totals are concentrated within the range of Δt_{mean} ± standard deviation (SD), and there is little difference in the amount of protein adsorption of BSA-PS particles within the Δt_{mean} ± SD range. At the same time, there are some extreme values in the total statistics. Although the extreme values deviate from Δt_{mean} ± SD, this can also provide us with some important information about individual particles. Therefore, the ratio of the number of BSA-PS particles outside the Δt_{mean} ± SD range to the total number of particles counted indirectly reflects the heterogeneity of the amount of protein adsorbed on the PS particles. As shown in Fig. 3c, the number of BSA-PS particles within the Δt_{mean} ± SD range as a proportion of the total number of particles counted for increasing adsorption times was 29 ± 2.5%, 39 ± 3%, 38 ± 6% and 32 ± 5.5%, respectively. As shown in Fig. 3d, the number of BSA-PS particles deviating from the range of Δt_{mean} ± SD as a proportion of the total number of particles counted under different adsorption times, was 71 ± 2.5%, 61 ± 3%, 62 ± 6% and 68 ± 5.5%, respectively. This provides us with heterogeneity information on the amount of adsorption on the BSA-PS particles for different adsorption times. This adsorption heterogeneity is related to the difference in particle size and the difference in surface chemistry of single particles, which affect the adsorption behavior of the particles [26]. Therefore, under the same conditions, information on the heterogeneity of physicochemical parameters at the surface of PS particles of the same size can be obtained indirectly through the heterogeneity of the BSA-PS particles.

4. Conclusion

In conclusion, we have demonstrated that single particle collision events at the tip of nanopipettes can be used for in situ monitoring of the heterogeneity of protein adsorption on single nanoparticles. Compared with other analytical methods, which can only describe the overall average adsorption behavior of nanoparticles, this method opens up the new possibility of obtaining information on the amount adsorbed on each single nanoparticle. More importantly, the method does not require any labeling on either nanoparticles or proteins.

Credit Autor statement

Ping Yu, Xiaohua He, Lanqun Mao conceived and designed the study. Wei Yi, Tienan Gao performed the experiments. Cong Xu and Tianyi Xiong Conducted the simulation. Wei Yi and Ping Yu wrote the manuscript. Cong Xu, Tianyi Xiong, Tienan Gao, Xiaohua He, Lanqun Mao reviewed and edited the manuscript. All authors read and approved the manuscript.

Declaration of Competing Interest

The authors declare that they have no known competing financial interests or personal relationships that could have appeared to influence the work reported in this paper.

Acknowledgments

We acknowledge financial support by Beijing Municipal Natural Science Foundation (JQ19009) and the National Natural Science Foundation of China (21775151 for P.Y. and 21790390, 21790391 for L.M. and 51773063 for X.H.).

Appendix A. Supplementary data

Supplementary data to this article can be found online at https://doi.org/10.1016/j.elecom.2020.106666.

References

[1] A. Vonarbourg, C. Passirani, P. Saulnier, J.P. Benoit, Biomaterials 27 (2006) 4356–4373.
[2] N. Feiner-Gracia, M. Beck, S. Pujals, S. Tosi, T. Mandal, C. Buske, M. Linden, L. Albertazzi, Small 13 (2017) 1701631.
[3] S.J. Soenen, P. Rivera-Gil, J.M. Montenegro, W.J. Parak, S.C. De Smedt, K. Braeckmans, Nano Today 6 (2011) 446–465.
[4] Z. Chen, P. Zhao, Z. Luo, M. Zheng, H. Tian, P. Gong, G. Gao, H. Pan, L. Liu, A. Ma, H. Cui, Y. Ma, L. Cai, ACS Nano 10 (2016) 10049–10057.
[5] M. Matsumoto, M. Matsusaki, M. Akashi, Macromol. Biosci. 14 (2014) 142–150.
[6] V. Forest, J. Pourchez, Nano Today 11 (2016) 700–703.
[7] S.R. Saptarshi, A. Duschl, A.L. Lopata, J. Nanobiotechnol. 11 (2013) 26.
[8] E. Izak-Nau, M. Voetz, S. Eiden, A. Duschl, V.F. Puntes, Part. Fibre Toxicol. 10 (2013) 56.
[9] J. Im, S. Lindsay, X. Wang, P. Zhang, ACS Nano 13 (2019) 6308–6318.
[10] C.B. Rosen, D. Rodriguez-Larrea, H. Bayley, Nat. Biotechnol. 32 (2014) 179.
[11] R. Gao, Y.L. Ying, Y.J. Li, Y.X. Hu, R.J. Yu, Y. Lin, Y.T. Long, Angew. Chem., Int. Edit. 57 (2018) 1011–1015.
[12] M. Zhou, Y. Yu, K. Hu, H.L. Xin, M.V. Mirkin, Anal. Chem. 89 (2017) 2880–2885.
[13] K. McKelvey, S.R. German, Y. Zhang, H.S. White, M.A. Edwards, Curr. Opin. Electrochem. 6 (2017) 4–9.
[14] P. Actis, M.M. Maalouf, H.J. Kim, A. Lohith, B. Vilozny, R.A. Seger, N. Pourmand, ACS Nano 8 (2013) 546–553.
[15] J. Zhang, J. Zhou, R. Pan, D. Jiang, J.D. Burgess, H.Y. Chen, ACS Sens. 3 (2018) 242–250.
[16] H. Liu, Q. Jiang, J. Pang, Z. Jiang, J. Cao, L. Ji, X. Xia, K. Wang, Adv. Funct. Mater. 28 (2018) 1703847.
[17] X. Lin, A.P. Ivanov, J.B. Edel, Chem. Sci. 8 (2017) 3905–3912.
[18] Y.L. Ying, R.J. Yu, Y.X. Hu, R. Gao, Y.T. Long, Chem. Commun. 53 (2017) 8620–8623.
[19] C. Yang, H. Wang, H. Tang, D. Zhao, Y. Li, Chem. Commun. 55 (2019) 10288–10291.
[20] R.J. Yu, Y.L. Ying, Y.X. Hu, R. Gao, Y.T. Long, Anal. Chem. 89 (2017) 8203–8206.
[21] H. Wang, H. Tang, C. Yang, Y. Li, Anal. Chem. 91 (2019) 7965–7970.
[22] Y. Liu, C. Xu, X. Chen, J. Wang, P. Yu, L. Mao, Electrochem. Commun. 89 (2018) 38–42.
[23] T. Li, X. He, K. Zhang, K. Wang, P. Yu, L. Mao, Chem. Sci. 7 (2016) 6365–6368.
[24] Y. Fu, H. Tokuhisa, L.A. Baker, Chem. Commun. (2009) 4877–4879.
[25] J.M. Rabanel, V. Adibnia, S.F. Tehrani, S. Sanche, P. Hildgen, X. Banquy, C. Ramassamy, Nanoscale 11 (2019) 383–406.
[26] C.D. Walkey, J.B. Olsen, H. Guo, A. Emili, W.C. Chan, J. Am. Chem. Soc. 134 (2012) 2139–2147.